# Equatorial Pacific Easterly Wind Surges and the Onset of La Niña Events*

ANDREW M. CHIODI AND D. E. HARRISON

*Joint Institute for the Study of the Atmosphere and Ocean, University of Washington, and NOAA/Pacific Marine Environmental Laboratory, Seattle, Washington*

(Manuscript received 25 March 2014, in final form 22 July 2014)

ABSTRACT

The processes responsible for the onset of La Niña events have not received the same attention as those responsible for the onset of El Niño events, for which westerly wind events (WWEs) in the tropical Pacific have been identified as important contributors. Results here show that synoptic-scale surface easterly wind surges (EWSs) play an important role in the onset of La Niña events, akin to the role of WWEs in the onset of El Niño events. It is found that EWSs are a substantial component of zonal wind stress variance along the equatorial Pacific. Using reanalysis wind stress fields, validated against buoy measurements, 340 EWS events are identified between 1986 and 2012. Their distributions in space, time, and El Niño–Southern Oscillation (ENSO) state are described. About 150 EWSs occur during ENSO-neutral conditions, during the months associated with La Niña initiation and growth (April–December). Composites of changes in sea surface temperature anomaly (SSTA) following these ~150 events show statistically significant cooling (0.1°–0.4°C) along the oceanic waveguide that persists for 2–3 months following the EWSs. Experiments with EWS forcing of an ocean general circulation model show SSTA patterns like those in the observations. It is suggested that EWSs play an important role in the onset of La Niña waveguide surface cooling and deserve additional study.

## 1. Introduction

The El Niño–Southern Oscillation (ENSO) is the primary mode of coupled ocean–atmosphere interannual variability in the tropical Pacific. ENSO has received widespread attention because it is the largest coupled mode of the planet after the seasonal cycle and diurnal cycle and because of its many associated effects on regional climate and ecosystems. ENSO's influence on seasonal weather anomalies can have predictable and socioeconomically important impacts in many regions around the globe (e.g., Goddard and Dilley 2005). Seasonal forecast skill in these regions depends upon skillful prediction of ENSO state and a usefully tight statistical relationship between ENSO and seasonal weather anomaly extremes (e.g., Chiodi and Harrison 2013). Although it was El Niño events, with their often-dramatic effects on the west coast of the Americas, that first gained wide attention, it is now clear that the societal impacts of La Niña events can be as consequential. So understanding the factors that control the onset and evolution of La Niña events is important. We describe here a mechanism that is responsible for the onset of ocean surface cooling in La Niña events.

The mechanisms responsible for ENSO events and how to improve predictions of them remain the focus of much effort, despite more than two decades of study. The quasi-oscillatory behavior of idealized coupled models (e.g., Schopf and Suarez 1988; Battisti and Hirst 1989; Neelin 1991; Jin 1997) show a clear potential for predictability over 1 yr ahead of the onset of an event (e.g., Neelin et al. 1998) that is often at odds with the observed history of ENSO initiation (Kessler and McPhaden 1995, 2002; Barnston et al. 2012). Progress has been made in identifying different aspects of Indo-Pacific variability that can help explain and better predict the observed timing of the El Niño and La Niña onsets (e.g., Clarke and Van Gorder 2003; see also Gutzler and Harrison 1987; Kug et al. 2005, 2010), but the history of the last decade makes it clear that

Denotes Open Access content.

*National Oceanic and Atmospheric Administration Contribution Number 2226 and National Oceanic and Atmospheric Administration/Pacific Marine Environmental Laboratory Contribution Number 4145.

*Corresponding author address:* Andrew Chiodi, NOAA/PMEL, Box 354925, 7600 Sand Point Way N.E., Seattle, WA 98115.
E-mail: andy.chiodi@noaa.gov

DOI: 10.1175/JCLI-D-14-00227.1

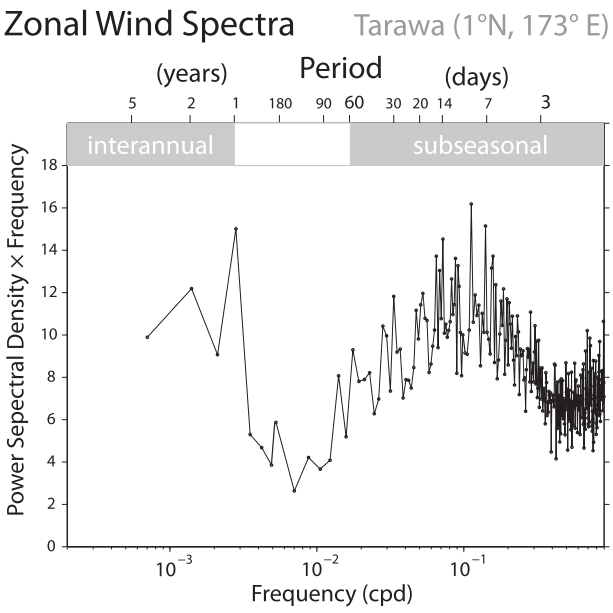


FIG. 1. Spectral density of variance of the zonal wind component measured at Tarawa (Republic of Kiribati) in energy preserving ($m^2 s^{-2}$) perspective. Data are from the Met Office subdaily station observations dataset, available through the Computational and Information Systems Laboratory (CISL) research data archive (at http://rda.ucar.edu/datasets/ds463.4: station ID 916100, period 1973–2011).

practical prediction experiences a spring prediction barrier for onset and prediction of the amplitude of events remains challenging (e.g., Jin et al. 2008; Barnston et al. 2012; Clarke 2014).

In addition to the delayed-oscillator coupled processes (e.g., Schopf and Suarez 1988; cf., Jin 1997), it is also clear that higher-frequency wind forcing also plays roles in ENSO (e.g., Keen 1982; Hartten 1996; Harrison and Vecchi 1997; Vecchi and Harrison 2000, hereinafter VH00; Perigaud and Cassou 2000; Belamari et al. 2003; Lengaigne et al. 2004; Harrison and Chiodi 2009; Kug et al. 2010; Chiodi et al. 2014). The zonal wind field in the central equatorial Pacific has a very distinctive spectrum, with high levels of variance at ENSO time scales (e.g., 3–8 yr), and a conspicuous peak at subseasonal (3–60 day) time scales. Harrison and Luther (1990) looked at surface wind data collected on tropical Pacific islands from 1949 to 1980 and found such spectra. Because there is considerable low-frequency variability of winds in the tropical Pacific, we first looked to see if zonal wind conditions have changed in this region since 1980. We find a similar spectrum at the same location. Figure 1, for example, shows the spectral density of variability of zonal wind at Tarawa (1°N, 173°W), over recent decades (1973–2011). The density of variance in Fig. 1 is plotted in ''energy preserving'' perspective so that the fraction of variance contained in each of the frequency bands is proportional to its value (*y*-axis position). As observed in previous decades by Harrison and Luther (1990), the frequency distribution of zonal wind energy at Tarawa exhibits a clear peak in the 3–60-day band, as well as strong levels of variability at ENSO time scales.

A large body of work now exists that shows how the westerly component of wind variability associated with this 3–60-day zonal wind energy peak is important to the initiation and maintenance of warm ENSO (El Niño) events (e.g., Luther et al. 1983; Harrison and Giese 1991; Hartten 1996; Harrison and Vecchi 1997; VH00; Harrison and Chiodi 2009; Chiodi et al. 2014). VH00 identified westerly wind events (WWEs) in the western to central tropical Pacific, with *e*-folding time scales of 6–7 days and amplitudes of 6–7 $m\,s^{-1}$ that, on average, precede observed sea surface temperature (SST) warming of a few to several tenths of a degree Celsius across the equatorial Pacific. Modeling studies indicate that it is anomalous zonal advection of the preexisting SST field that is primarily responsible for the initial warming of the sea surface temperature anomaly (SSTA; Schopf and Harrison 1983; Harrison and Schopf 1984; Giese and Harrison 1991; Kindle and Phoebus 1995; Lengaigne et al. 2002). Low-vertical-mode Kelvin pulses cause deepening of the equatorial Pacific thermocline along with upper-ocean easterly current anomalies and have also been observed following WWEs by McPhaden (2004) and Kessler and McPhaden (1995). Wind stress anomalies from a single WWE have been shown to drive SSTAs like those seen in the observations when applied to ocean models (e.g., Kindle and Phoebus 1995; Giese and Harrison 1991; Richardson et al. 1999; Belamari et al. 2003) and even drive mature El Niño events when applied to realistic ocean models with timing and frequency like that seen over recent El Niño events (Harrison and Chiodi 2009).

WWEs are not random noise, nor are they spawned by Madden–Julian oscillation (MJO) events (Chiodi et al. 2014). Rather, their characteristics are a function of the large-scale environment in which they form. The chances of a WWE increase as ENSO transitions from its cool (La Niña) to warm (El Niño) phase, making the effects of WWEs on the tropical Pacific an important part of its ''slow'' (i.e., multiseason) transition to El Niño (Perigaud and Cassou 2000; Lengaigne et al. 2003, 2004; Eisenman et al. 2005; Vecchi et al. 2006; Gebbie et al. 2007; Gebbie and Tziperman 2009a,b).

Visual inspection of, say, the Tarawa zonal wind time series reveals the WWEs very directly (see also Luther et al. 1983). Although there is also easterly wind variability at the 3–60-day time scale, until now the effects of these easterlies have not received the same level of attention as WWEs (cf., Eisenman et al. 2005; Kug et al.

2010), even though equatorial wave and surface current anomalies are as easily forced by easterly stress anomalies as they are by westerly stress anomalies. We show here that there are easterly wind surges (EWSs) of oceanic dynamic and thermodynamic importance, which reveal themselves when zonal wind stress is considered. It is necessary to look at wind stress rather than wind for EWSs because a modest increase in easterly wind on top of prevailing easterly trades can lead to a dynamically important increase in stress.

To determine the characteristics of EWSs and their relationship to the equatorial Pacific cooling that occurs in the onset of La Niña events, we examine estimates of equatorial Pacific surface wind stress for periods of statistically significant and meaningful increases in easterly surface momentum flux that last at least a few days. We identify EWS events using an objective definition and, after describing their distribution with longitude across the tropical Pacific, as well as time of year, we perform a composite analysis to examine the changes in tropical Pacific SSTA that follow them. The EWS wind stress composites are also applied to a realistic ocean general circulation model in order to compare the observed SSTA changes with those produced by the EWSs in the model. The distribution of EWS events with ENSO state is also examined and discussed.

## 2. Methodology

### a. Data

Gridded, $1° \times 1°$ surface wind stress estimates ($\tau$) were obtained from the global atmospheric Interim European Centre for Medium-Range Weather Forecasts (ECMWF) Re-Analysis (ERA-Interim; Dee et al. 2011). Daily averages were calculated from 3-hourly data available online (at http://apps.ecmwf.int/datasets/data/interim_full_daily/).

A second set of surface wind stress estimates were also obtained from the Tropical Atmosphere Ocean (TAO) project for verification purposes. In this case, surface wind stress at the TAO buoy locations is estimated from moored-buoy meteorological observations using the Coupled Ocean–Atmosphere Response Experiment (COARE) 3.0b algorithm (Fairall et al. 2003), as described by Cronin et al. (2006).

For SST information, we use the Optimum Interpolation Sea Surface Temperature version 2 (OISSTv2) dataset described by Reynolds et al. (2002) and provided by National Oceanic and Atmospheric Administration/Office of Oceanic and Atmospheric Research/Earth System Research Laboratory/Physical Sciences Division (NOAA/OAR/ESRL/PSD), Boulder, Colorado (available at http://www.esrl.noaa.gov/psd/). OISST data are available on a $1° \times 1°$ grid at weekly resolution. For this study, the weekly data were interpolated to daily resolution to estimate the changes in SSTA that occur on subseasonal time scales [following Chiodi et al. (2014) and Harrison and Chiodi (2009)].

For the observed variables ($\tau$ and SST), daily average anomalies are calculated based on linear interpolation of the respective monthly average climatology (the full study period, 1986–2012, is used as the climatological base period).

### b. Ocean model

The ocean model used herein is based on the long-standing NOAA primitive equation OGCM in the tropical Pacific form first set up by Philander and Seigel (1985). The configuration used here is based on the NOAA/Geophysical Fluid Dynamics Laboratory (GFDL) Modular Ocean Model, version 4 (MOM4; Griffies et al. 2003). The global version of MOM4 is the oceanic component of the GFDL Climate Model, version 2 (Gnanadesikan et al. 2006), and a tropical Pacific version of the model has been used recently to successfully describe the seasonal cycle of the near-surface tropical Pacific by Harrison et al. (2009) and to study the effects of WWE wind stress anomalies by Harrison and Chiodi (2009), as well as the effects of WWEs and the MJO (Chiodi et al. 2014). Model SSTA is determined in this case following the procedure of Harrison et al. (2009), and it is computed as the difference between a control run, forced by climatologically varying wind stress, and a second run forced with the climatological plus anomaly wind stress.

### c. Easterly surge identification

There have been numerous studies of the characteristics of WWEs (e.g., Keen 1982; Giese and Harrison 1990, 1991; Harrison and Vecchi 1997; Richardson et al. 1999; VH00; Belamari et al. 2003; Lengaigne et al. 2004; Seiki and Takayabu 2007; Harrison and Chiodi 2009; Gebbie and Tziperman 2009a). We shall here follow an approach similar to that of VH00, except that we use zonal wind stress, rather than zonal wind anomaly information, to identify easterly wind stress surges. Our focus will be limited here to the easterly surges that occur in the near-equatorial region since we are interested in the oceanic waveguide changes that follow them.

We focus here on easterly wind stress surges identified in daily averaged and waveguide-averaged (5°S–5°N averaged) wind stress anomalies across the Pacific (120°E–80°W). We identify ''EWS regions'' as regions of at least 25° of longitude that maintain (or exceed) a spatially averaged easterly wind stress anomaly of

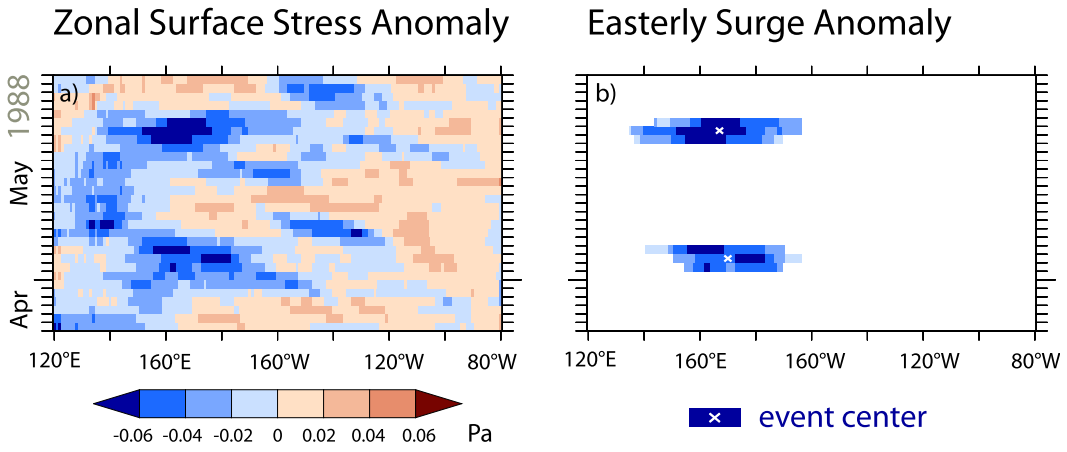


FIG. 2. (a) Equatorial Pacific zonal surface stress anomaly averaged over 5°S–5°N in late April–May 1988. (b) Easterly wind surge events (shaded regions), with event centers marked by the white crosses.

$<-0.045$ Pa for at least three consecutive days. The region over which the anomaly exceeds the threshold may differ day by day but must overlap the previous such region; this allows events to grow in zonal length or propagate eastward/westward.

Our choice of the $-0.045$ Pa anomaly threshold was informed by a preliminary inspection of the westerly wind stress anomalies associated with the near-equatorial WWEs identified using the VH00 WWE definition. The VH00 WWE definition requires a 10-m wind anomaly of $2\,\mathrm{m\,s^{-1}}$ or greater for three or more consecutive days, averaged over the given WWE-definition region. The equatorially centered W-, C-, and E-type WWE-definition regions have bounds of 5°S–5°N in the meridional direction and 130°–155°E, 155°E–180°, and 180°–150°W, respectively, in the zonal direction. The wind stress anomalies seen over the three initial days of the VH00-identified WWEs (period 1986–2012) range from 0.033 to 0.43 Pa, depending on which type of WWE was considered (W, C, or E). It bears noting, however, that VH00 used a different wind dataset (the 12-hourly ECMWF 10-m wind operational forecast record) than we do. Inspection has shown that, although the basic structure (e.g., sign) of daily average zonal wind anomalies is usually in agreement between these two datasets, stronger subseasonal time-scale peaks are typically seen in the ERA-Interim dataset (which we find to be more closely matched to the TAO buoy-measured winds throughout the study period) than the ECMWF operational dataset. Thus, using the ERA-Interim winds typically yields more WWEs over a given time than using the ECMWF operational forecast winds. Accordingly, we also considered the effects of using a $2.5\,\mathrm{m\,s^{-1}}$, rather than $2.0\,\mathrm{m\,s^{-1}}$, zonal wind anomaly threshold for identifying WWEs based on ERA-Interim wind data, after finding that this combination yields a WWE frequency that more closely matches the original VH00 results. In the $2.5\,\mathrm{m\,s^{-1}}$ ERA-Interim wind data case, the average WWE-associated wind stress ranges from 0.038 to 0.047 Pa, yielding a total (including the $2.0\,\mathrm{m\,s^{-1}}$ results) WWE-associated range of 0.033–0.047 Pa. We tried using EWS zonal stress anomaly thresholds ranging from $-0.03$ to $-0.05$ Pa and found that the SSTA change results (as discussed below) remains qualitatively similar regardless of the threshold chosen; by this, we mean that the SSTA-change pattern discussed below remains similar, albeit with somewhat stronger (weaker) peak amplitudes in the higher- (lower-) threshold cases. Sensitivity of the results to this threshold is discussed more below in the modeling section. The $-0.045$ Pa threshold was chosen after finding that this yields an average EWS frequency that roughly matches (at about 1 per month) the all-time-averaged WWE frequencies previously reported (VH00; Harrison and Chiodi 2009) for WWEs.

A case example of the identification of two such EWSs in the spring of 1988 is provided in Fig. 2, wherein the full 5°S–5°N daily averaged zonal wind stress anomaly is shaded in Fig. 2a and just the portions identified as EWS wind stress anomalies are shaded in Fig. 2b. Once the easterly surge anomalies are identified, we also identify an event center (shown by the white crosses) in a manner analogous to the classical determination of an object's center of mass in two dimensions, with the dimensions in this case being longitude and time. Specifically, the center longitude of the event ($X$) is defined as

$$X = \sum_{i,j} \frac{x_{i,j} \cdot \tau_{i,j}}{\tau_{i,j}}$$

and the center day ($T$) of the event is

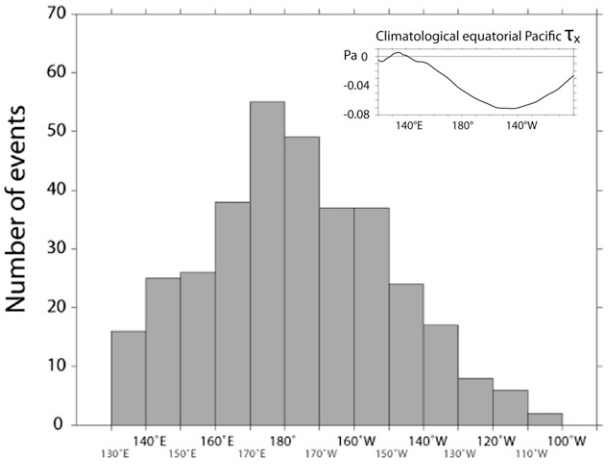


FIG. 3. Longitudinal distribution of easterly surges. Zonal wind stress averaged over the period 1986–2012 and 5°S–5°N is shown in the inset.

$$T = \sum_{i,j} \frac{t_{i,j} \cdot \tau_{i,j}}{\tau_{i,j}},$$

where $\tau_{i,j}$ is the identified surge wind stress anomaly at longitude $x_{i,j}$ and time $t_{i,j}$. The summation is in this case carried out over (just) the time and space of the identified easterly surge, as shown by the shaded region(s) in Fig. 2b.

## 3. Results

### a. EWS event distribution with season and longitude

We begin with the distributions of the 340 EWSs identified between 1986 and 2012 in time and space. Their center longitude distribution across the equatorial Pacific (Fig. 3) peaks near the international date line (170°E–170°W contains the most EWSs per degree longitude and 32% of the total number of EWSs). However, substantial numbers of EWSs also occur both east and west of the peak region; 75% of the EWSs occur in the region bounded by 150°E and 145°W. There are a few events in the far western Pacific and even fewer in the far eastern Pacific.

To look for systematic longitudinal propagation, we also examined the characteristics of the center longitudes of each day within each EWS (a linear least squares fit to each set of center longitudes was used to estimate event propagation). Lower-frequency wind variability in the tropical Indo-Pacific has often exhibited zonal propagation (e.g., Madden and Julian 1972; Gutzler and Harrison 1987), although no systematic propagation was found for the average WWEs (Harrison and Vecchi 1997). No systematic propagation of EWSs was found either; the number of events that moved a few degrees west over the duration of the event are roughly matched in number by those that moved few degrees east. Some EWSs also show very little displacement over the event, with most events propagating less than 4° longitude per day (i.e., $<5.1\,\mathrm{m\,s^{-1}}$) and 30% (16%) moving less than 2° (1°).

The climatological zonal wind stress in the equatorial Pacific is shown in the inset panel of Fig. 3. The near–date line peak in numbers of easterly surges occurs roughly halfway between the longitudes, where the easterlies are at their climatological peak (near 145°W), and the far western Pacific (e.g., 120°–150°E), where the climatological average zonal wind component is nearer to zero. Because wind stress is roughly proportional to the square of zonal wind speed in this case, reaching the event criteria of −0.045 Pa requires a stronger easterly wind speed anomaly in the far western Pacific than in the eastern central Pacific. For example, compared to the bulk parameterization (e.g., Large and Pond 1981) wind stresses computed from climatological winds measured by TAO/Triangle Trans-Ocean Buoy Network (TRITON) buoys along the equator at 147°E, 180°, and 140°W (with mean zonal winds of −0.78, −4.2, and $-5.6\,\mathrm{m\,s^{-1}}$, respectively), the zonal wind speeds would have to increase (become a larger negative number) by roughly another 5, 3, and $2.5\,\mathrm{m\,s^{-1}}$, respectively, in order to reach the −0.045 Pa threshold at these three locations. The large number of events seen near the date line to the western Pacific regions therefore serves as a reminder that these are areas of especially active subseasonal wind variability.

The zonal extents of the EWSs (i.e., the maximum length of the region with average zonal wind stress anomaly $<-0.045$ Pa) range from 27° to 81° longitude, with a mean of 50°. The average duration (number of above-threshold days) of the EWS events is 6 days, with the longest lasting 28 days. It is unusual for events to remain above threshold ($<-0.045$ Pa) for more than two weeks; only 7 of the 340 EWSs (2%) do so.

The distribution of EWS events by month is shown in Fig. 4. The fewest number of events were observed in April and the most in August. However, we found the observed month-to-month differences to be not very statistically significant based on a Monte Carlo simulation in which the 340 events were randomly distributed across the 1986–2012 period (none reach the 95% confidence level). The hypothesis that these events actually have an equal chance to occur regardless of season is consistent (at the 95% confidence level) with their observed distribution over the period considered.

### b. Composites of EWS wind stress

The composite average EWS wind stress anomaly, based on the 340 identified surge events, is shown in

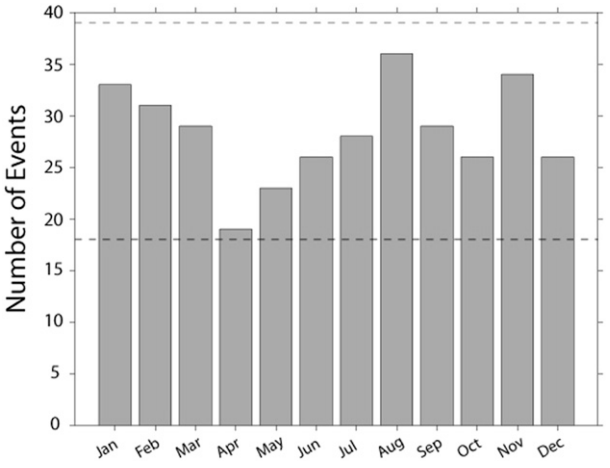


FIG. 4. Distribution of easterly surge events by month over the 1986–2012 period. The dashed lines indicate the 95% confidence interval for the (null) hypothesis test that event frequency is independent of season.

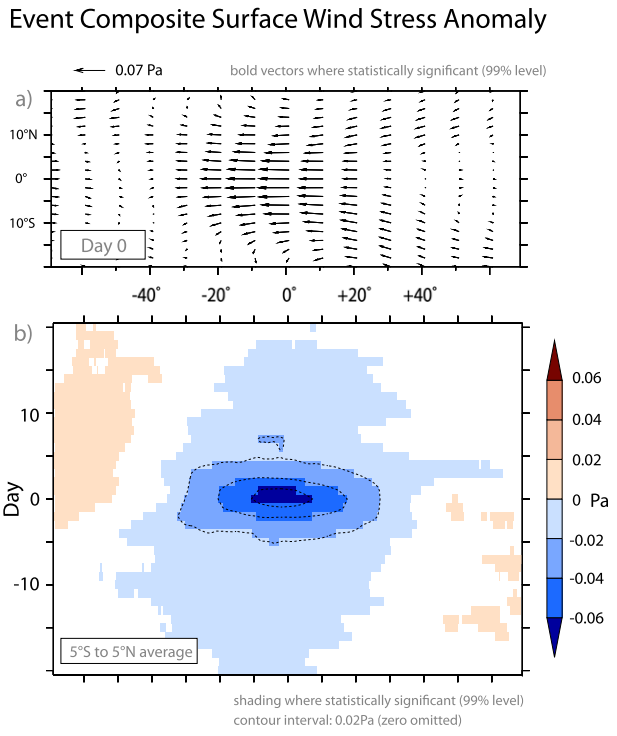


FIG. 5. (top) Composite average center day wind stress anomaly based on the 340 identified easterly surge events. (bottom) Time–longitude plot of the easterly surge zonal wind stress anomaly composite.

Fig. 5. To construct this composite, day 0 is taken to be the center day for each event and the center longitude of each event is assigned to be "0" longitude. The Monte Carlo–based methods used to determine the statistical significance of the composite wind stress anomalies take this mapping into account (see appendix A). The day-0 wind stress anomaly composite (Fig. 5, top) shows a peak daily average wind stress anomaly in excess of −0.06 Pa within about 10° of the center of the event. This amplitude of wind stress anomaly is highly statistically significant (>99% level) in this case. Somewhat weaker but still statistically significant (from −0.02 to −0.06 Pa) easterlies also extend another 20° longitude or so from the event center.

A time–longitude plot of the equatorial portion (5°–5°N) of this composite shows easterly anomalies greater than 0.02 Pa in amplitude from roughly day −5 to day +5, near the center longitude of the event (Fig. 5, bottom). Peak easterly anomalies greater than 0.06 Pa in amplitude occur here only near the center longitude and only for a few days, whereas smaller amplitude yet still statistically significant easterlies can be seen over most of the day −20 to day +20 interval shown. Some of this low amplitude, yet statistically significant, easterly tail may be due to the occurrence of other easterly surge events in the same vicinity. We have also split the total number of EWSs into equal thirds based on their center longitude before compositing them and found similar (within 10% of one another) peak, center-day wind stress anomaly amplitudes in each case but stronger easterly tails (several days removed from the center day) in the composite based on the center (and to lesser extent western) third than eastern third. Since the longitude distribution is least concentrated in the eastern third, this can be taken as being consistent with the view that some of the easterly tail is due to other close-by surge events. Weaker but still statistically significant westerlies can also be seen in the bottom panel of Fig. 5, located far afield (>40°) of the easterly surges. The combination of westerlies in the far western Pacific and easterlies in the central Pacific indicates that the near-surface zonal wind is typically convergent to the west of the easterly surge locations.

The structure of the EWS wind stress anomaly composite looking along its center longitude and (separately) day 0 is plotted in Fig. 6, where we have also shown these aspects of a WWE wind stress anomaly composite for comparison (i.e., the C type based on a 2.5 m $s^{-1}$ threshold VH00-type definition and ERA-Interim winds: period 1986–2012). It is clear that the EWS composite has a wind stress anomaly structure that is roughly similar in amplitude, duration and zonal extent to the inverse of a WWE wind stress anomaly composite.

### c. *Observed SSTA changes following easterly surges*

We focus here on the SSTA changes following EWSs that occur during ENSO-neutral conditions and in the months associated with La Niña cooling, since we are

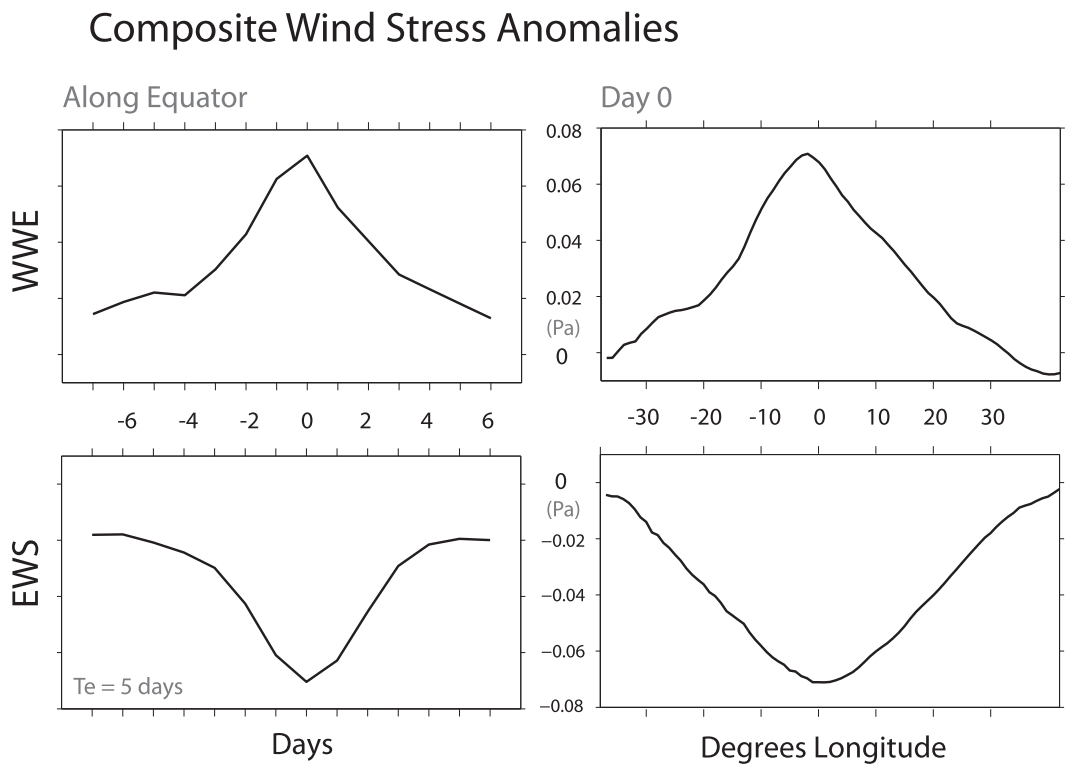


FIG. 6. Comparison of WWE and EWS wind stress anomaly composites for the period 1986–2012.

interested in the role of EWSs in the onset of La Niña events. Following Harrison and Vecchi (1997) (see also VH00; Harrison and Chiodi 2009; Chiodi et al. 2014), we define ENSO neutral as the times in which the Niño-3 index has an amplitude less than 0.75°C (|Niño-3| < 0.75°C). The ENSO composites of Larkin and Harrison (2002) have previously shown the months from April to December to be the time of year when La Niña events have typically grown out of neutral background to nearly mature stages. Thus, we focus on the effects of the events that occur in these neutral-onset conditions (all April–December days with |Niño-3| < 0.75°C).

Out of the 340 original events, we identify 148 that occur in these neutral-onset conditions. The composite average +20-day change in SSTA following them, computed here as the change in SSTA from 20 days before to 20 days after the center day of the event [as in Harrison and Vecchi (1997), except for changes following EWSs], (see the top panel of Fig. 8) where a small-amplitude (<0.1°C) but nonetheless statistically significant cooling is seen in the equatorial central Pacific from roughly 180° to 140°W (see appendix A for statistical significance estimation methods). This central Pacific cooling persists into the +40- and +60-day composites (Fig. 7, middle two panels), whereas larger-amplitude (~0.3°C) and statistically significant cooling patterns develop further east in the equatorial Pacific cold tongue region during this time. Statistically significant cooling like that seen in cold tongue region in the +60-day composite persists to day +80 (Fig. 7, bottom), at which point most of the oceanic waveguide region west of 160°W has experienced a significant drop in SSTA of a few tenths of a degree Celsius. It is clear that, on average, the cold tongue region is cooled following these EWSs.

### d. *Model experiment: Effects of a single EWS*

We hypothesize that the cooling seen following the easterly surges is mainly driven by the momentum flux anomalies they impart on the equatorial Pacific oceanic waveguide region and the ocean circulation anomalies that follow. We test this hypothesis in the context of a primitive equation ocean general circulation model by applying the easterly surge wind stress composite to the model after it has been spun up to realistic climatological conditions [see Harrison et al. (2009) for a comparison of the model-reproduced and observed climatology].

For consistency with the SSTA change composite described in the previous section, the wind stress composite applied to the model is in this case on the same set of 148 EWS events, and the compositing is done relative to geographic (rather than event-centered) longitude. In this case, the wind stress anomaly composite has lower

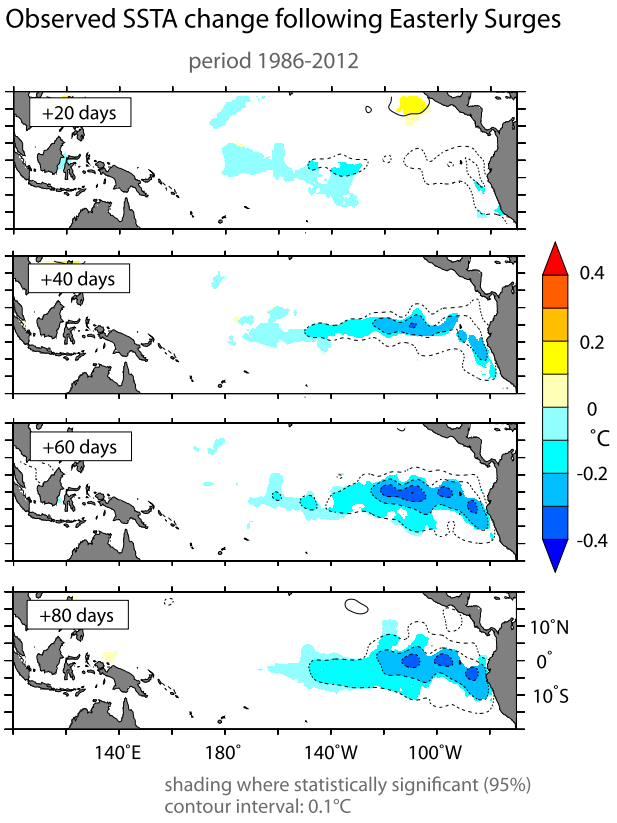


FIG. 7. Observed SSTA changes following the easterly surge events that occur in ENSO-neutral conditions, during the times of year associated with the initiation of La Niña events.

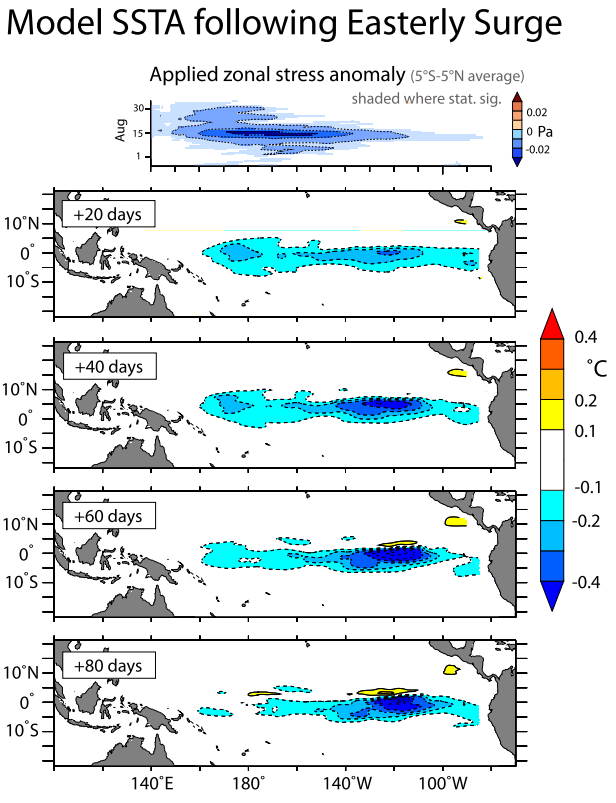


FIG. 8. (top) Easterly surge wind stress composite (time–longitude perspective). (bottom) Snapshots of model SSTA following the application of the easterly surge wind stress.

peak amplitude than is seen in the EWS event-centered case, but broader zonal extent (cf., Fig. 5 and top panel of Fig. 8) so that the zonally integrated easterly momentum flux remains comparable in each case. A time–longitude plot of the EWS composite wind stress anomaly applied to the model is shown in the top panel of Fig. 8. We have chosen to apply the surge composite centered in August since the highest number of events was observed then. Prior to running the model experiment, we compared the ERA-Interim-based composite with wind stress estimated from the TAO buoy data and found a tendency for the peak ERA-Interim wind stress composite anomalies, at the times of the EWSs, to exceed TAO results by roughly 20% (see Table B1). Since we expect a higher level of accuracy from the buoy-based estimates, we adjusted the ERA-Interim composite amplitude to TAO by multiplying the ERA-Interim composite (as shown in Fig. 8, top) by a factor of 0.8 before applying it to the model. Not adjusting the ERA-Interim composite to TAO would result in stronger model cooling than is described below.

The model SSTAs following the TAO-adjusted EWS show that the surge wind stress anomaly drives cooling anomalies along the oceanic waveguide with amplitude and pattern broadly similar to those seen in the observations (cf. Figs. 7 and 8). For example, at day +20, some cooling is seen near the date line that persists, albeit with somewhat diminished amplitude, to day +60. Also, a larger-amplitude (several tenths of a degree Celsius) cooling anomaly develops to the east of the near–date line region during this time, which persists to day +80. There are also differences between the observations and model results. Perhaps the largest difference is that the model experiment is unable to reproduce the large cooling amplitudes observed in the far eastern equatorial Pacific (i.e., east of 100°W). We expect that this occurs in large part because the details of the ocean circulation and associated temperature changes seen off the coast of South America are not well reproduced in the model. Nonetheless, the model and observations agree that cooling occurs in this region of the ocean. Across the majority of the oceanic waveguide (from western to central equatorial Pacific), we find good consistency between the observed and modeled SSTA changes following EWSs.

We have also repeated this pair of analyses (observed SSTA-change composites and EWS-driven model experiments) with the subset of EWSs that occur in just

warm–neutral ENSO conditions (0.0°C < Niño-3 < 0.75°C). It is well known that the easterly trades typically strengthen as the tropical Pacific transitions to La Niña. It was suggested in review that because many of the 148 EWS events occur when ENSO SSTA is moderately cool (more on this below) some of the cooling seen in the composited SSTA changes, as well as some of the strength of the EWS wind stress composites, could be contributed by a low-frequency strengthening of the easterly trades caused by (already) cool ENSO SSTA. In warm–neutral conditions, however, the effect of ENSO SSTA on the zonal equatorial winds should, if anything, drive warming rather than cooling. Yet, we find that even in the warm–neutral set of results (Fig. 9) the waveguide cooling amplitudes seen in both the model and observations are at least as large as in the full neutral case. This strongly suggests that it is the EWS wind stress anomaly that drives the observed cooling patterns.

We have also experimented with adding event centered, rather than geographically fixed, wind stress anomaly composites to the model (as is discussed more in the following section). These experiments have confirmed that EWS-centered wind stress anomaly composites may be added to the model with longitude centers from 165°E to 150°W without substantially changing the oceanic waveguide cooling amplitudes from those seen in Fig. 8.

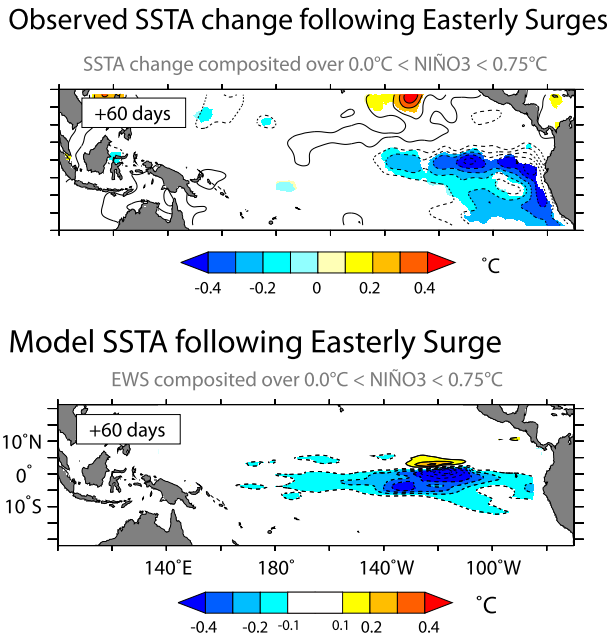


FIG. 9. (top) The +60-day composite of SSTA changes observed following the EWSs that occur in warm–neutral (0°C < Niño-3 < 0.75°C) conditions. Composite anomalies that are significant at the 95% level are shaded. (bottom) The +60-day model SSTA following an applied EWS. In this case, the applied EWS wind stress composite is based on just those events that occurred in warm–neutral conditions.

### *e. Model experiment: Effects of a series of EWSs*

The total number of EWSs identified (340) divided by the time span considered (324 months) gives us an average frequency of very nearly 1 EWS per month over this time. Since the system spends most of its time in the ENSO-neutral (as defined herein) state, this frequency is also roughly representative of the average frequency of EWSs observed then (as is confirmed below).

In this section, we examine the effects of adding series of EWSs at a frequency of 1 per month. To do this, multiple EWSs are applied to the model from April to December of the experiment year, with center days selected using Monte Carlo methods that produce (on average) 1 EWS per month. In the experiment described in this section, nine EWS wind stress composites are applied to the ocean model, one for each month from April to December. The center longitudes of the EWSs were selected randomly from the observed distribution (shown in Fig. 3). As in the experiment described in the previous section, the wind stress anomaly magnitudes are adjusted to the TAO-based composites by multiplying them by a factor of 0.8 before applying them to the ocean model.

A time–longitude plot of the equatorial wind stress anomaly applied to the ocean model in the first experiment is shown in the left panel of Fig. 10. The resulting equatorial model SSTA is shown in the center panel of Fig. 10, and the average model SSTA over the Niño-3.4 region is also shown on the right side of this figure for reference. In this case, the Niño-3.4 region SSTA cools to approximately the −0.5°C level shortly (within about a month) after the occurrence of the first EWS in early April and, aided by three more EWSs that occur from late April to July, the Niño-3.4 index maintains a value near −0.5°C until mid-August. A slight relaxation toward 0°C occurs in the time between the last of these three EWSs (in early July) and the next EWS (which occurs outside of the Niño-3.4 region) in late August. Following this relaxation, the succession of three more EWSs from late August to the end of September again cool the Niño-3.4 region to the −0.5°C level and beyond, as peak cooling of about −0.75°C is seen shortly after two more EWSs occur near the beginning of November, both located just within the western edge of the Niño-3.4 region (an optimal location for producing effects on the Niño-3.4 region, which has 170°W as its western boundary). However, this enhanced cooling does not last long. After the last of the November EWSs occurs, Niño-3.4 again relaxes toward zero, reaching −0.5°C in late December on a warming (relaxing) trend. In summary, based on this experiment, persistent cooling of

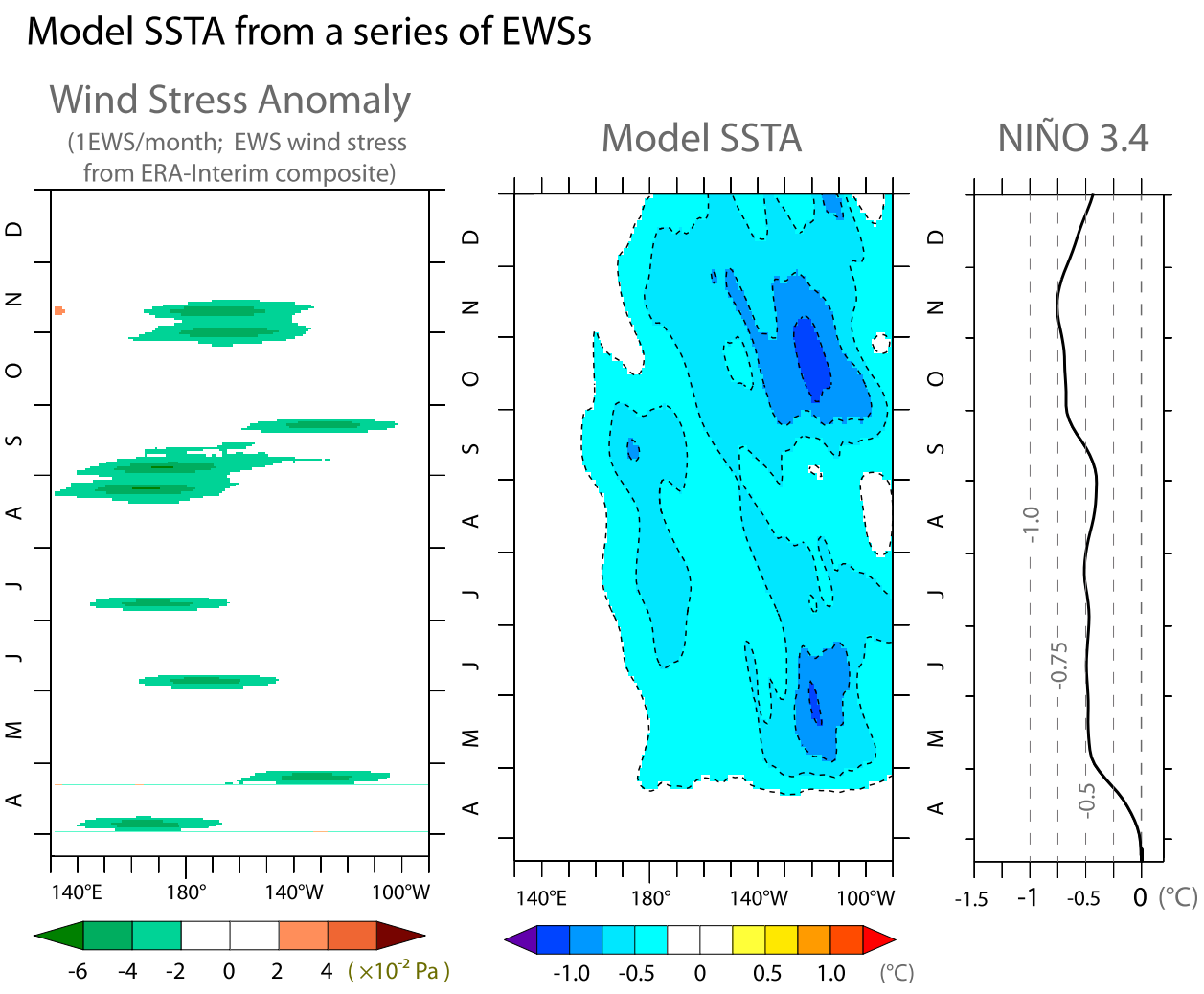


FIG. 10. (left) Wind stress anomaly applied to the ocean model (5°S–5°N averaged). In this case, the ERA-Interim-based EWS composite is applied nine times from April to December. (center) Model SSTA (5°S–5°N averaged). (right) Model SSTA averaged over the Niño-3.4 region.

about 0.5°C less than the climatological average can be expected from (just) a one-per-month series of EWSs that occurs from April to December, in the absence of other types of ENSO forcing.

We have repeated this experiment based on results obtained using two other candidate EWS-identification threshold values of −0.04 and −0.05 Pa (the base case discussed here uses −0.045 Pa). We found that when the higher (lower) magnitude threshold is used, the number of EWSs identified decreases (increases) but the composite wind stress anomaly also increases (decreases). The changes in EWS frequency and wind stress anomaly amplitude in these cases amount to 20%–30% of the base-case values used herein. We find that when that when these changes are included in the experiment—for example, applying a somewhat stronger EWSs composite less frequently—their effects basically cancel one another and the amounts of SSTA cooling produced in the modified experiments is very comparable to what is shown in Fig. 10.

### *f. The distribution of EWS with ENSO SSTA*

As mentioned in the introduction, previous studies on WWEs have found that their likelihood of occurrence depends on the anomaly state of the tropical Pacific, with WWEs becoming more frequent as the tropical Pacific moves into warm ENSO conditions (e.g., VH00; Gebbie and Tziperman 2009a; Chiodi et al. 2014). This knowledge has motivated us to look at whether the chances of seeing an EWS also depend on ENSO state.

Figure 11 shows the distribution of surge events with the center day value of the Niño-3.4 and (to nearly the

same effect) Niño-3 index. The vast majority (95% and 94% for Niño-3.4 and Niño-3, respectively) of events occur when these ENSO SSTA indices are below the +1°C (warm ENSO) level (Fig. 11, top), with the range from 0° to −1°C being the anomaly conditions containing the largest percentages of identified EWSs (43% and 49% of the total, based on Niño-3.4 and Niño-3, respectively). It should be recognized, however, that ENSO does not spend an equal amount of time in each range of SSTA values depicted in the top panel of Fig. 11. Dividing the number of events seen in each SSTA bin in the top panel of Fig. 11 by the number of days spent in each bin yields the event frequency distribution shown in the bottom panel of Fig. 11. From this perspective, it becomes apparent that there is a rather steady increase in event frequency moving from the +1°C to La Niña state. For example, the chances of seeing an EWS roughly double as the Niño-3.4 index moves from +1° to −1°C and then roughly double again moving from −1° to −2°C.

The easterly surge event frequency in the very warm ENSO regime also appears to be in some cases near or even greater than what is observed in the neutral regime. Inspection shows that each EWS that occurred in the >+2°C regime did so during the later stages of the large El Niño event of 1997/98. The increased central Pacific easterlies seen then have previously been shown to play an important role in the abrupt termination of the 1997/98 El Niño (e.g., Harrison and Vecchi 1999; Takayabu et al. 1999). Although notable in this respect, the EWSs that occur when Niño-3.4 is greater than +2°C comprise only 2% of total number of EWSs identified, which makes the robustness of their event frequency statistics in these conditions unclear. During our study period, Niño-3.4 spent most days (72%) in the range from −1° to +1°C, where the clear result is that there is a substantial increase in the frequency of EWSs as the tropical Pacific transitions from its moderately warm to moderately cool anomaly state.

Following previous studies that examined the way WWEs are distributed with ENSO state (e.g., VH00; Gebbie and Tziperman 2009a), we have herein identified (easterly surge) wind events based on departures from the seasonal climatology. It was suggested in review that this method of counting EWS events is susceptible to bias introduced by fundamentally low-frequency (e.g., interannual time scale) wind variations that, for example, might strengthen the easterly trades during La Niña and thereby lead to an over counting of EWS in the La Niña state. On the other hand, just as the trade winds in the western equatorial Pacific were observed to weaken before El Niño events not in a uniform but rather in an episodic manner (Luther et al. 1983), so too does the strengthening of the zonal trade winds

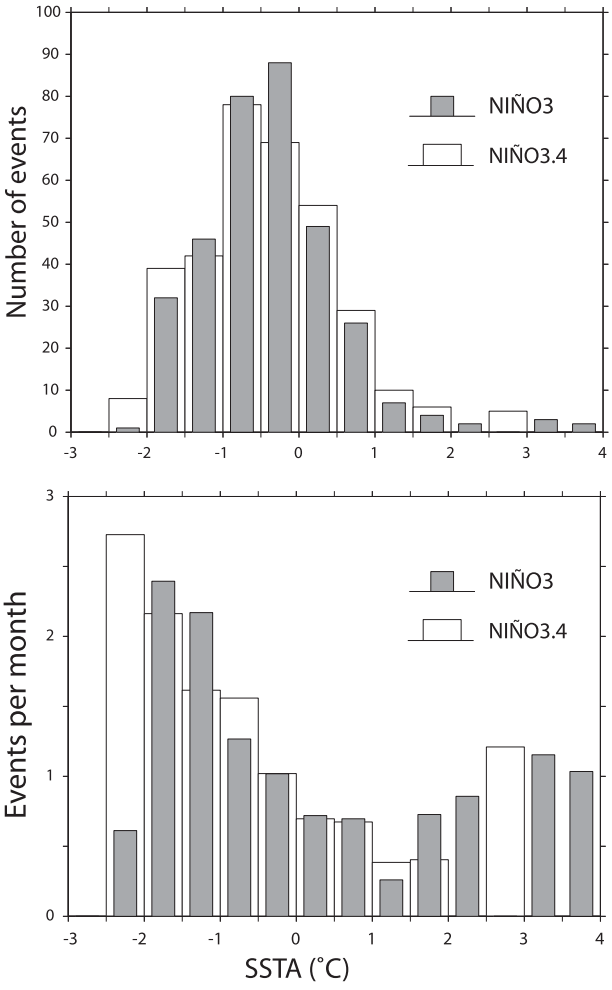


FIG. 11. (top) Distribution of the numbers of easterly surge events by ENSO state. (bottom) Distribution of easterly surge event frequency by ENSO state.

along the equator prior to La Niña have an episodic character (e.g., Fig. 12). This suggests the possibility that longer time scale (e.g., interannual) averages of the zonal wind may themselves be strongly affected by asymmetries in the distribution of EWS events with ENSO state. To further investigate this perspective, we have computed La Niña composite zonal wind stress anomalies [following the methods of Larkin and Harrison (2002)] based on the ERA-Interim wind stress as well as a second wind stress field that was constructed by just applying the EWS composite (as shown in Fig. 5) at the 340 identified EWS center days/longitudes. Doing this, we found that there is sufficient momentum contributed by these EWS events to account for the strengthening of easterly wind stress anomalies that is seen during the onset and growth stages of La Niña events (not shown for brevity). The question of whether the strengthening of easterly trades during La Niña is best thought of

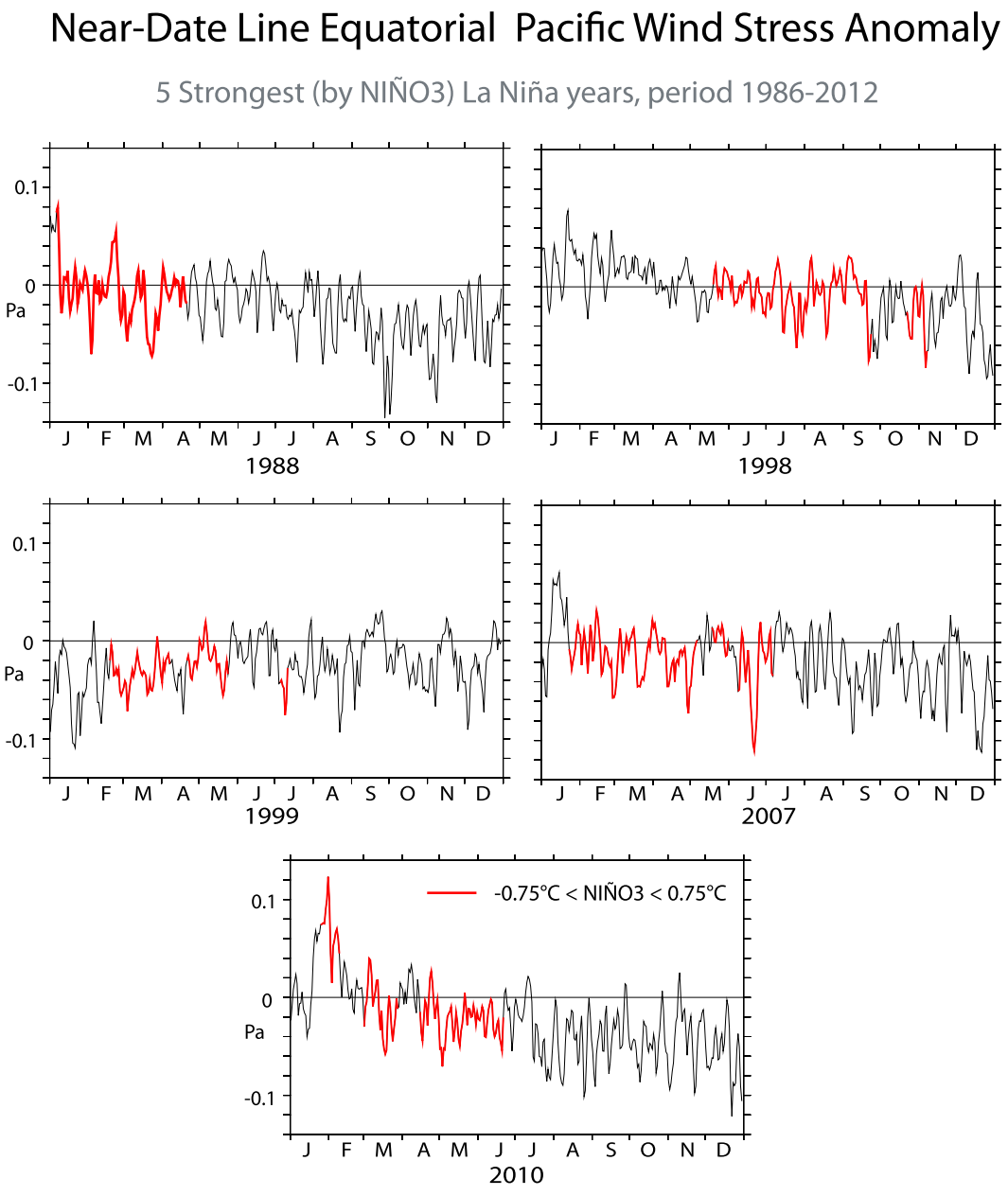


FIG. 12. Zonal wind stress anomaly averaged over 5°S–5°N, 170°E–170°W during year 0 of the five strongest (based on ENSO SSTA) La Niña years in the 1986–2012 period. Wind stress here is from ERA-Interim. Times in which |Niño-3| < 0.75°C are denoted by the red curves.

as a fundamentally low-frequency (interannual) process or if instead the strengthening is accomplished episodically through easterly surge events that become more frequent as ENSO state transitions from neutral to La Niña conditions deserves further attention. In the next section, we use the ocean model to examine what kind of SSTA response should be expected in the scenario that EWS events become more frequent as the system cools.

### *g. The effects of a series of EWSs with a ramp up in frequency*

This second EWS-series experiment is like that described in section 3e, except in this case we modify the Monte Carlo methods such that the prescribed EWS frequency increases linearly from 1 to 2 per month moving from April to December of the experiment year. The wind stress anomaly applied to the model in this

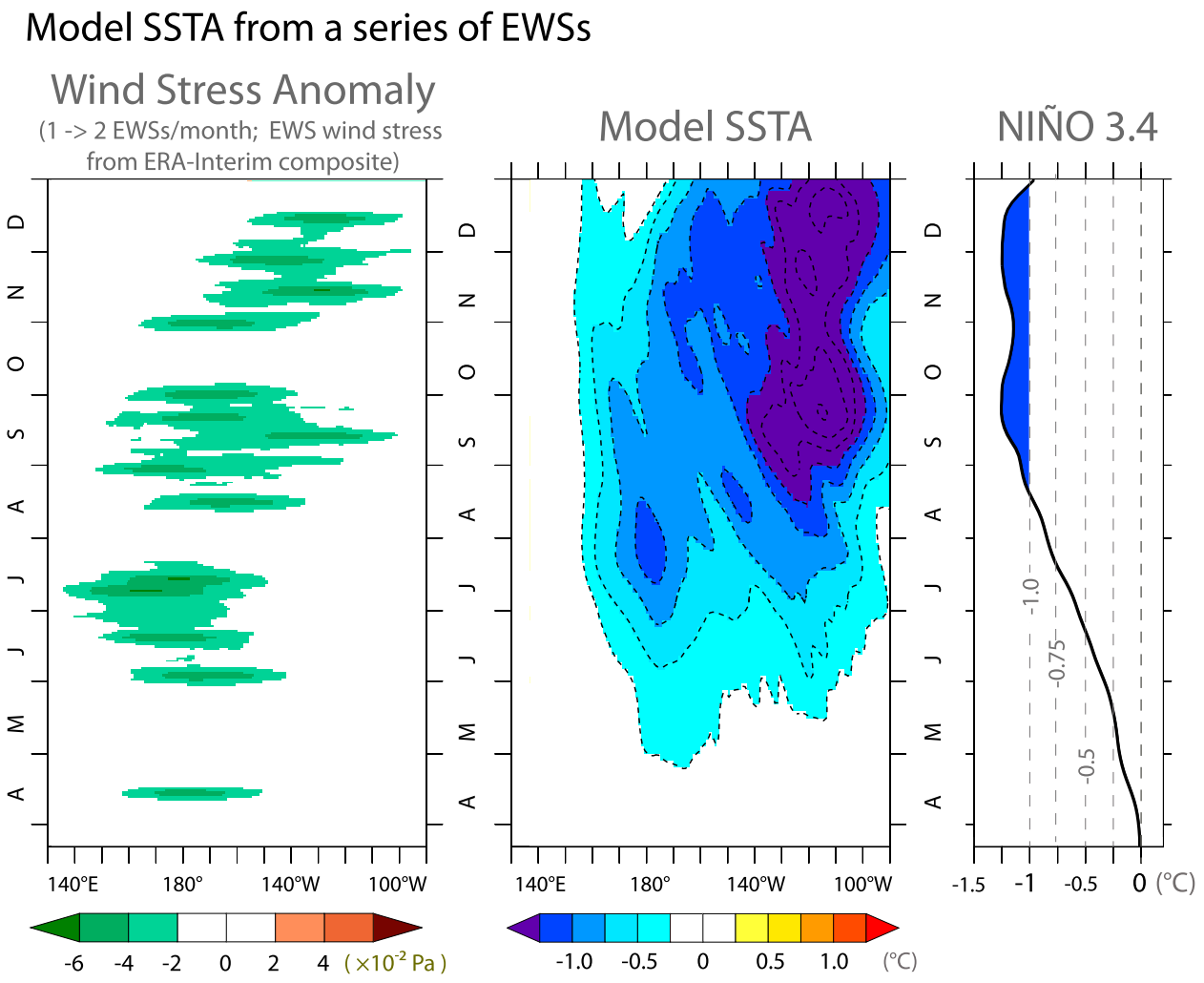


FIG. 13. (left) Wind stress anomaly applied to the ocean model (5°S–5°N averaged). In this case, the ERA-Interim-based EWS composite is applied 14 times from April to December. (center) Model SSTA (5°S–5°N averaged). (right) Model SSTA averaged over the Niño-3.4 region.

experiment is shown in Fig. 13 (left). In this case, 14 EWSs are applied from April to December in total; although their timing retains a stochastic character, the prescribed ramp up in frequency from 1 to 2 per month over this period is evident. As before, the equatorially averaged model SSTA is shown in the center panel of Fig. 13 and the average over the Niño-3.4 regions is plotted in the right panel. What is most notable here, in comparison with the previous experiment's results, is that now, because of the ramp up in EWS frequency, the Niño-3.4 region remains cooler than −1°C for the vast majority of the September–December period (the October–December average Niño-3.4 value is −1.2°C in this case).

These results show that, in this model, the effects of EWS wind stress anomalies alone, when applied with their average frequency (~1 per month), are enough to push the tropical Pacific toward its cool ENSO state and, should this EWS frequency increase (as it is observed to do based on our identification methods following cooling of the central tropical Pacific region), the combined effects of (just) the applied EWSs are enough to drive a La Niña event.

## 4. Summary and discussion

Despite their relatively brief duration, westerly wind events have been shown to be an important factor in the onset of El Niño surface warming over the equatorial Pacific cold tongue region. While corresponding events of easterly wind are not as obvious in the wind time series, we have shown here that counterparts to the WWEs

exist as surges in the easterly wind stress field; we call these easterly wind surges (EWSs). We have introduced an objective definition for EWSs that identifies 340 events in the 1986–2012 period. On average, then, there is roughly 1 EWS per month. The average duration, amplitude (in wind stress anomaly), and zonal extent of EWSs are roughly similar to those of WWEs.

A key motivator of this work was to find out if EWSs also play a role in the onset of cold tongue cooling in La Niña events comparable to the role of WWEs in the onset of warming in El Niño events. We find that statistically significant decreases in SSTA follow the EWS events that occur in ENSO-neutral conditions during the months of the year associated with La Niña onset and growth. This is based on composites of the ~150 events found at these times in the 1986–2012 period, which show that cooling amplitudes up to 0.4°C persist in the equatorial cold tongue region for 2–3 months after the EWSs subside. This amount of cooling is comparable in magnitude and zonal extent to the warming that similar studies indicate follows a typical WWE.

The application of (a single) EWS composite wind stress anomaly to an ocean model produces cooling anomalies that resemble the cooling patterns seen in the observations following a single EWS event. Notwithstanding some model deficiencies seen along the far eastern Pacific coast, the cooling amplitudes in the model following the application of a single EWS are at least as large as those in the observations. This holds even if the set of EWSs considered is restricted to just those that occur just in warm–neutral ENSO conditions: that is, before La Niña–type SSTA cooling is evident (i.e., 0°C < Niño-3 < 0.75°C). This strongly suggests EWSs provide a mechanism for La Niña onset.

We find that distribution of EWSs varies with ENSO state (e.g., Niño-3 or Niño-3.4) such that their average frequency over conditions cooler than −1°C (~2 per month) is roughly double the full study period average. This suggests to us that much of the strengthening of the easterly trade winds during La Niña results from EWSs becoming more frequent as ENSO SSTA cools. On the other hand, if this strengthening of the easterly trades is best thought of as a fundamentally lower-frequency (interannual) process, then our methods of identifying EWS in La Niña would be biased high. We suggest that the hypothesis that the La Niña strengthening of the trades is accomplished episodically is one that deserves more attention than it has received up to this point.

Model experiments show that the application of a series of EWSs that includes the observed ramp up in EWS frequency is sufficient to drive a La Niña–type SSTA pattern in the model (e.g., end of calendar year Niño-3.4 SSTA < −1°C, lasting for 3 months). In this scenario, starting from near-neutral, springtime conditions, the occurrence of an EWS typically drives waveguide cooling that, in turn, makes EWSs more likely to occur (and WWEs less likely to occur; VH00; Gebbie and Tziperman 2009a). The coupled Gill (1980) mechanism is then carried out in this phase of La Niña by EWSs.

Even without the ramp in frequency, however, a series of ~1 per month EWSs is sufficient to drive the model about halfway to a La Niña–type anomaly state (e.g., Niño-3.4 SSTA in the range from −0.5° to −0.75°C). This strongly suggests that EWS events can make an important contribution to both the initial onset and subsequent growth of La Niña events.

These results provide an initial step in understanding the role that EWSs play in ENSO, but much remains to be learned. One obvious question motivated by these results is whether indices tracking early ENSO stage EWS activity can be found that add to the existing strategies for bridging the springtime prediction barrier (cf. Clarke and Van Gorder 2003; Kug et al. 2010). Also, the role that EWSs play as La Niña events mature and decay (e.g., WWEs have been shown by VH00 to maintain waveguide warmth but not necessarily add to it in warm ENSO conditions) or occur in other anomaly states, perhaps in close succession to WWEs, or even at the mature stages of El Niño, is deserving of attention. Although, at first glance, EWSs and WWEs appear to have similar (though oppositely signed) wind stress characteristics, whether or not there are asymmetries in their distribution or frequency that contribute to asymmetry in the longer-term average zonal wind stress characteristics associated with El Niño and La Niña (e.g., Ohba and Ueda 2009; Okumura et al. 2011; Dommenget et al. 2013) may also be deserving of further attention. Also, as discussed above, the reasons for the observed tendency for EWSs to increase in frequency as the tropical Pacific moves from moderately warm to cool anomaly states is deserving of future study. We suggest that improving our understanding of the sources and predictability of EWSs offers a means to improve our understanding of these aspects of La Niña onset.

*Acknowledgments.* This manuscript benefitted from the considerable proof reading skills of S. Bigley. The authors thank M. Lengaigne and an anonymous reviewer for their thoughtful reviews and helpful comments, as well as M. Cronin for help obtaining (and efforts to compute make publicly available) the wind stress anomalies based on the TAO/TRITON buoys. This publication is (partially) funded by the Joint Institute for the Study of the Atmosphere and Ocean (JISAO) under NOAA Cooperative Agreement NA10OAR4320148 and funded by the Climate Observations and Monitoring Program, National Oceanic and

TABLE B1. Comparison of ERA-Interim and TAO/TRITON-based wind stress estimates (Pa) at the equatorial TAO buoy locations (listed in the first column; 0° lat in each case). The values listed in the first five columns are computed over all times with buoy measurements and are as follows: (i) root-mean-square TAO minus ERA-Interim difference; (ii) time-average TAO value; (iii) time-average ERA-Interim value; (iv) TAO standard deviation (STD); and (v) ERA-Interim standard deviation. The final three columns are based on daily average anomaly values with base periods consisting of all times with buoy measurements at each location. These columns list the EWS center day (day 0) wind stress anomaly using TAO, the ERA-Interim center day EWS wind stress anomaly, and the percent difference between the TAO and ERA-Interim composites [(TAO − ERA-Interim)/ERA-Interim], respectively.

| | RMS TAO − ERA-Interim | Mean TAO | Mean ERA | STD TAO | STD ERA | EWS composite with TAO | EWS composite with ERA-Interim | Composite diff |
|---|---|---|---|---|---|---|---|---|
| 147°E | 0.0123 | −0.0047 | −0.0077 | 0.0297 | 0.0346 | −0.0100 | −0.0123 | 19% |
| 156°E | 0.0124 | −0.0064 | −0.0103 | 0.0352 | 0.0391 | −0.0176 | −0.0221 | 20% |
| 165°E | 0.0151 | −0.0117 | −0.0168 | 0.0423 | 0.0440 | −0.0296 | −0.0330 | 10% |
| 180° | 0.0133 | −0.0483 | −0.0574 | 0.0371 | 0.0386 | −0.0274 | −0.0308 | 11% |
| 155°W | 0.0170 | −0.0578 | −0.0726 | 0.0348 | 0.0368 | −0.0175 | −0.0255 | 32% |
| 140°W | 0.0160 | −0.0556 | −0.0697 | 0.0316 | 0.0342 | −0.0075 | −0.0121 | 38% |
| 125°W | 0.0162 | −0.0397 | −0.0572 | 0.0246 | 0.0291 | −0.0013 | −0.0040 | 67% |
| 110°W | 0.0142 | −0.0290 | −0.0401 | 0.0229 | 0.0240 | $-1.26 \times 10^{-4}$ | $-2.0 \times 10^{-4}$ | — |
| 95°W | 0.0105 | −0.0142 | −0.0143 | 0.0163 | 0.0163 | 0.0022 | $2.95 \times 10^{-4}$ | — |

Atmospheric Administration, U.S. Department of Commerce. Support was also provided by the NOAA/Pacific Marine Environmental Laboratory (PMEL).

## APPENDIX A

### Bootstrap Monte Carlo Methods

This appendix briefly describes the methods used to determine the statistical significances of the composite anomalies shown in Fig. 5 (wind stress) and Fig. 7 (SSTA change). To do this, we apply bootstrap Monte Carlo procedures like those previously described, in general terms, by Efron and Tibshirani (1991). In this case, the approach involves simulating the composite analysis procedure using a randomly sampled (with replacement) set of EWS times and locations rather than the observed EWS times and locations. Repetition ($N$ = 1000) and sorting of the (many) repeated simulation results then allows the likelihood that the observed anomaly amplitudes might be reached based on chance alone to be determined.

For each repetition of the bootstrap procedure, a simulation set of EWS times is chosen randomly such that the total number of EWSs entering into the composite remains the same (i.e., 340). We employ a procedure to do this that randomly selects times such that their distribution with Niño-3.4 (on average) matches that shown in the bottom panel of Fig. 11. In this way, any variability in wind stress (or SSTA change) that is linearly related to ENSO is accounted for in the bootstrap confidence intervals; the composite anomaly amplitudes must surpass the effects of any such linear relationship to reach statistical significance.

The wind stress case also involves a spatial mapping from geographic to EWS-centered composite grids and so requires an additional step to account for this. In this case, for each repetition of the bootstrap procedure we also randomly select 340 EWS longitudes from the observed distribution (e.g., Fig. 3) so that the effects of using EWS-centered longitudinal coordinates in the actual composites match those reproduced in the bootstrap procedure.

## APPENDIX B

### TAO/TRITON versus ERA-Interim Easterly Wind Surge Wind Stress Comparison

Table B1 compares various aspects of near-equatorial wind stress as it is estimated from TAO/TRITON buoy-based measurements (using the COARE 3.0b algorithm) and in the ERA-Interim dataset. In the ERA-Interim case, only wind stress estimates in the grid cells centered closest to the given TAO buoy locations are considered and only over times for which TAO buoy observations are available. The most relevant result here, for our purposes, is that the ERA-Interim dataset tends to overestimate, relative to TAO, the amplitude of the easterly wind stress anomalies associated with the EWSs in the regions where the EWSs typically occur; the average percent difference between the TAO- and ERA-Interim-based EWS composites from 147°E to 155°W (140°W) is 18% (22%), with the ERA-Interim case predicting the larger-amplitude (though same sign) easterly wind stress anomaly.

## REFERENCES

Barnston, A. G., M. K. Tippett, M. L. L'Heureux, S. Li, and D. G. DeWitt, 2012: Skill of real-time seasonal ENSO model predictions

during 2002–11: Is our capability increasing? *Bull. Amer. Meteor. Soc.,* **93,** 631–651, doi:10.1175/BAMS-D-11-00111.1.

Battisti, D. S., and A. C. Hirst, 1989: Interannual variability in the tropical ocean-atmosphere system: Influence of the basic state, ocean geometry and nonlinearity. *J. Atmos. Sci.,* **46,** 1687–1712, doi:10.1175/1520-0469(1989)046<1687:IVIATA>2.0.CO;2.

Belamari, S., J. L. Redelsperger, and M. Pontaud, 2003: Dynamic role of a westerly wind burst in triggering an equatorial Pacific warm event. *J. Climate,* **16,** 1869–1890, doi:10.1175/1520-0442(2003)016<1869:DROAWW>2.0.CO;2.

Chiodi, A. M., and D. E. Harrison, 2013: El Niño impacts on seasonal U.S. atmospheric circulation, temperature, and precipitation anomalies: The OLR-event perspective. *J. Climate,* **26,** 822–837, doi:10.1175/JCLI-D-12-00097.1.

——, ——, and G. A. Vecchi, 2014: Subseasonal atmospheric variability and El Niño waveguide warming: Observed effects of the Madden–Julian oscillation and westerly wind events. *J. Climate,* **27,** 3619–3642, doi:10.1175/JCLI-D-13-00547.1.

Clarke, A. J., 2014: El Niño physics and El Niño predictability. *Annu. Rev. Mar. Sci.,* **6,** 79–99, doi:10.1146/annurev-marine-010213-135026.

——, and S. Van Gorder, 2003: Improving El Niño prediction using a space-time integration of Indo-Pacific winds and equatorial Pacific upper ocean heat content. *Geophys. Res. Lett.,* **30,** 1399, doi:10.1029/2002GL016673.

Cronin, M. F., C. Fairall, and M. J. McPhaden, 2006: An assessment of buoy derived and numerical weather prediction surface heat fluxes in the tropical Pacific. *J. Geophys. Res.,* **111,** C06038.

Dee, D. P., and Coauthors, 2011: The ERA-Interim reanalysis: Configuration and performance of the data assimilation system. *Quart. J. Roy. Meteor. Soc.,* **137,** 553–597, doi:10.1002/qj.828.

Dommenget, D., T. Bayr, and C. Frauen, 2013: Analysis of the non-linearity in the pattern and time evolution of El Niño southern oscillation. *Climate Dyn.,* **40,** 2825–2847, doi:10.1007/s00382-012-1475-0.

Efron, B., and R. Tibshirani, 1991: Statistical data analysis in the computer age. *Science,* **253,** 390–395, doi:10.1126/science.253.5018.390.

Eisenman, I., L. Yu, and E. Tziperman, 2005: Westerly wind bursts: ENSO's tail rather than the dog? *J. Climate,* **18,** 5224–5238, doi:10.1175/JCLI3588.1.

Fairall, C. W., E. F. Bradley, J. E. Hare, A. A. Grachev, and J. B. Edson, 2003: Bulk parameterization of air–sea fluxes: Updates and verification for the COARE algorithm. *J. Climate,* **16,** 571–591, doi:10.1175/1520-0442(2003)016<0571:BPOASF>2.0.CO;2.

Gebbie, G., and E. Tziperman, 2009a: Predictability of SST-modulated westerly wind bursts. *J. Climate,* **22,** 3894–3909, doi:10.1175/2009JCLI2516.1.

——, and ——, 2009b: Incorporating a semi-stochastic model of ocean-modulated westerly wind bursts into an ENSO prediction model. *Theor. Appl. Climatol.,* **97,** doi:10.1007/s00704-008-0069-6.

——, I. Eisenman, A. Wittenberg, and E. Tziperman, 2007: Modulation of westerly wind bursts by sea surface temperature: A semi-stochastic feedback for ENSO. *J. Atmos. Sci.,* **64,** 3281–3295, doi:10.1175/JAS4029.1.

Giese, B. S., and D. E. Harrison, 1990: Aspects of the Kelvin wave response to episodic wind forcing. *J. Geophys. Res.,* **95,** 7289–7312, doi:10.1029/JC095iC05p07289.

——, and ——, 1991: Eastern equatorial Pacific response to three composite westerly wind types. *J. Geophys. Res.,* **96,** 3239–3248, doi:10.1029/90JC01861.

Gill, A. E., 1980: Some simple solutions for heat-induced tropical circulation. *Quart. J. Roy. Meteor. Soc.,* **106,** 447–462, doi:10.1002/qj.49710644905.

Gnanadesikan, A., and Coauthors, 2006: GFDL's CM2 global coupled climate models. Part II: The baseline ocean simulation. *J. Climate,* **19,** 675–697, doi:10.1175/JCLI3630.1.

Goddard, L., and M. Dilley, 2005: El Niño: Catastrophe or opportunity. *J. Climate,* **18,** 651–665, doi:10.1175/JCLI-3277.1.

Griffies, S. M., M. J. Harrison, R. C. Pacanowski, and A. Rosati, 2003: A technical guide to MOM 4. NOAA/Geophysical Fluid Dynamics Laboratory Ocean Group Tech. Rep. 5, 295 pp.

Gutzler, D. S., and D. E. Harrison, 1987: The structure and evolution of seasonal wind anomalies over the near-equatorial eastern Indian and western Pacific oceans. *Mon. Wea. Rev.,* **115,** 169–192, doi:10.1175/1520-0493(1987)115<0169:TSAEOS>2.0.CO;2.

Harrison, D. E., and P. S. Schopf, 1984: Kelvin-wave-induced anomalous advection and the onset of surface warming in El Niño events. *Mon. Wea. Rev.,* **112,** 923–933, doi:10.1175/1520-0493(1984)112<0923:KWIAAA>2.0.CO;2.

——, and D. S. Luther, 1990: Surface winds from tropical Pacific islands—Climatological statistics. *J. Climate,* **3,** 251–271, doi:10.1175/1520-0442(1990)003<0251:SWFTPI>2.0.CO;2.

——, and B. S. Giese, 1991: Episodes of surface westerly winds as observed from islands in the western tropical Pacific. *J. Geophys. Res.,* **96,** 3221–3237, doi:10.1029/90JC01775.

——, and G. A. Vecchi, 1997: Westerly wind events in the tropical Pacific. *J. Climate,* **10,** 3131–3156, doi:10.1175/1520-0442(1997)010<3131:WWEITT>2.0.CO;2.

——, and ——, 1999: On the termination of El Niño. *Geophys. Res. Lett.,* **26,** 1593–1596, doi:10.1029/1999GL900316.

——, and A. M. Chiodi, 2009: Pre- and post-1997/98 westerly wind events and equatorial Pacific cold tongue warming. *J. Climate,* **22,** 568–581, doi:10.1175/2008JCLI2270.1.

——, A. Chiodi, and G. Vecchi, 2009: Effects of surface forcing on the seasonal cycle of the eastern equatorial Pacific. *J. Mar. Res.,* **67,** 701–729, doi:10.1357/002224009792006179.

Hartten, L. M., 1996: Synoptic settings of westerly wind bursts. *J. Geophys. Res.,* **101,** 16 997–17 019, doi:10.1029/96JD00030.

Jin, E. K., and Coauthors, 2008: Current status of ENSO prediction skill in coupled ocean-atmosphere models. *Climate Dyn.,* **31,** 647–664, doi:10.1007/s00382-008-0397-3.

Jin, F.-F., 1997: An equatorial ocean recharge paradigm for ENSO. Part I: Conceptual model. *J. Atmos. Sci.,* **54,** 811–829, doi:10.1175/1520-0469(1997)054<0811:AEORPF>2.0.CO;2.

Keen, R. A., 1982: The role of cross-equatorial cyclone pairs in the Southern Oscillation. *Mon. Wea. Rev.,* **110,** 1405–1416, doi:10.1175/1520-0493(1982)110<1405:TROCET>2.0.CO;2.

Kessler, W. S., and M. J. McPhaden, 1995: Oceanic equatorial waves and the 1991–93 El Niño. *J. Climate,* **8,** 1757–1774, doi:10.1175/1520-0442(1995)008<1757:OEWATE>2.0.CO;2.

——, and ——, 2002: Is ENSO a cycle or a series of events? *Geophys. Res. Lett.,* **29,** 2125, doi:10.1029/2002GL015924.

Kindle, J. C., and P. A. Phoebus, 1995: The ocean response to operational westerly wind bursts during the 1991–1992 El Niño. *J. Geophys. Res.,* **100,** 4893–4920, doi:10.1029/94JC02392.

Kug, J.-S., S.-I. An, F.-F. Jin, and I.-S. Kang, 2005: Preconditions for El Niño and La Niña onsets and their relation to the Indian Ocean. *Geophys. Res. Lett.,* **32,** L05706, doi:10.1029/2004GL021674.

——, K.-P. Sooraj, T. Li, and F.-F. Jin, 2010: Precursors of the El Niño/La Niña onset and their interrelationship. *J. Geophys. Res.,* **115,** D05106, doi:10.1029/2009JD012861.

Large, W., and S. Pond, 1981: Open ocean flux measurements in moderate to strong winds. *J. Phys. Oceanogr.,* **11,** 324–336, doi:10.1175/1520-0485(1981)011<0324:OOMFMI>2.0.CO;2.

Larkin, N. K., and D. E. Harrison, 2002: ENSO warm (El Niño) and cold (La Niña) event life cycles: Ocean surface anomaly patterns, their symmetries, asymmetries, and implications. *J. Climate,* **15,** 1118–1140, doi:10.1175/1520-0442(2002)015<1118:EWENOA>2.0.CO;2.

Lengaigne, M., J.-P. Boulanger, C. Menkes, S. Masson, G. Madec, and P. Delecluse, 2002: Ocean response to the March 1997 westerly wind event. *J. Geophys. Res.,* **107,** 8015, doi:10.1029/2001JC000841.

——, ——, ——, G. Madec, P. Delecluse, E. Guilyardi, and J. M. Slingo, 2003: The March 1997 westerly wind event and the onset of the 1997/98 El Niño: Understanding the role of the atmospheric response. *J. Climate,* **16,** 3330–3343, doi:10.1175/1520-0442(2003)016<3330:TMWWEA>2.0.CO;2.

——, E. Guilyardi, J. P. Boulanger, C. Menkes, P. Delecluse, P. Inness, J. Cole, and J. Slingo, 2004: Triggering of El Niño by westerly wind events in a coupled general circulation model. *Climate Dyn.,* **23,** 601–620, doi:10.1007/s00382-004-0457-2.

Luther, D. S., D. E. Harrison, and R. A. Knox, 1983: Zonal winds in the central equatorial Pacific and El Niño. *Science,* **222,** 327–330, doi:10.1126/science.222.4621.327.

Madden, R. A., and P. R. Julian, 1972: Description of global-scale circulation cells in the tropics with a 40–50 day period. *J. Atmos. Sci.,* **29,** 1109–1123, doi:10.1175/1520-0469(1972)029<1109:DOGSCC>2.0.CO;2.

McPhaden, M. J., 2004: Evolution of the 2002/03 El Niño. *Bull. Amer. Meteor. Soc.,* **85,** 677–695, doi:10.1175/BAMS-85-5-677.

Neelin, J. D., 1991: The slow sea surface temperature mode and fast-wave limit: Analytic theory for tropical interannual oscillations and experiments in a hybrid coupled model. *J. Atmos. Sci.,* **48,** 584–606, doi:10.1175/1520-0469(1991)048<0584:TSSSTM>2.0.CO;2.

——, D. S. Battisti, A. C. Hirst, F.-F. Jin, Y. Wakata, T. Yamagata, and S. E. Zebiak, 1998: ENSO theory. *J. Geophys. Res.,* **103,** 14 261–14 290, doi:10.1029/97JC03424.

Ohba, M., and H. Ueda, 2009: Role of nonlinear atmospheric response to SST on the asymmetric transition process of ENSO. *J. Climate,* **22,** 177–192, doi:10.1175/2008JCLI2334.1.

Okumura, Y. M., M. Ohba, C. Deser, and H. Ueda, 2011: A proposed mechanism for the asymmetric duration of El Niño and La Nina. *J. Climate,* **24,** 3822–3829, doi:10.1175/2011JCLI3999.1.

Perigaud, C. M., and C. Cassou, 2000: Importance of oceanic decadal trends and westerly wind bursts for forecasting El Niño. *Geophys. Res. Lett.,* **27,** 389–392, doi:10.1029/1999GL010781.

Philander, S. G. H., and A. D. Seigel, 1985: Simulation of El Niño of 1982–1983. *Coupled Ocean-Atmosphere Models,* J. Nihoul, Ed., Elsevier, 517–541.

Reynolds, R. W., N. A. Rayner, T. M. Smith, D. C. Stokes, and W. Wang, 2002: An improved in situ and satellite SST analysis for climate. *J. Climate,* **15,** 1609–1625, doi:10.1175/1520-0442(2002)015<1609:AIISAS>2.0.CO;2.

Richardson, R. A., I. Ginis, and L. M. Rothstein, 1999: A numerical investigation of the local ocean response to westerly wind burst forcing in the western equatorial Pacific. *J. Phys. Oceanogr.,* **29,** 1334–1352, doi:10.1175/1520-0485(1999)029<1334:ANIOTL>2.0.CO;2.

Schopf, P. S., and D. E. Harrison, 1983: On equatorial waves and El Niño I. Influence of initial states on wave-induced currents and warming. *J. Phys. Oceanogr.,* **13,** 936–948, doi:10.1175/1520-0485(1983)013<0936:OEWAEN>2.0.CO;2.

——, and M. J. Suarez, 1988: Vacillations in a coupled ocean-atmosphere model. *J. Atmos. Sci.,* **45,** 549–566, doi:10.1175/1520-0469(1988)045<0549:VIACOM>2.0.CO;2.

Seiki, A., and Y. N. Takayabu, 2007: Westerly wind bursts and their relationship with intraseasonal variations and ENSO. Part I: Statistics. *Mon. Wea. Rev.,* **135,** 3325–3345, doi:10.1175/MWR3477.1.

Takayabu, Y. N., T. Iguchi, M. Kachi, A. Shibata, and H. Kanzawa, 1999: Abrupt termination of the 1997-98 El Niño in response to a Madden-Julian oscillation. *Nature,* **402,** 279–282, doi:10.1038/46254.

Vecchi, G. A., and D. E. Harrison, 2000: Tropical Pacific sea surface temperature anomalies, El Niño, and equatorial westerly wind events. *J. Climate,* **13,** 1814–1830, doi:10.1175/1520-0442(2000)013<1814:TPSSTA>2.0.CO;2.

——, A. T. Wittenberg, and A. Rosati, 2006: Reassessing the role of stochastic forcing in the 1997–1998 El Niño. *Geophys. Res. Lett.,* **33,** L01706, doi:10.1029/2005GL024738.